Continuous Flow Deformability-Based Separation of Circulating Tumor Cells Using Microfluidic Ratchets

*Emily S. Park, Chao Jin, Quan Guo, Richard R. Ang, Simon P. Duffy, Kerryn Matthews, Arun Azad, Hamidreza Abdi, Tilman Todenhöfer, Jenny Bazov, Kim N. Chi, Peter C. Black, and Hongshen Ma**

***C**irculating tumor cells (CTCs) offer tremendous potential for the detection and characterization of cancer. A key challenge for their isolation and subsequent analysis is the extreme rarity of these cells in circulation. Here, a novel label-free method is described to enrich viable CTCs directly from whole blood based on their distinct deformability relative to hematological cells. This mechanism leverages the deformation of single cells through tapered micrometer scale constrictions using oscillatory flow in order to generate a ratcheting effect that produces distinct flow paths for CTCs, leukocytes, and erythrocytes. A label-free separation of circulating tumor cells from whole blood is demonstrated, where target cells can be separated from background cells based on deformability despite their nearly identical size. In doping experiments, this microfluidic device is able to capture >90% of cancer cells from unprocessed whole blood to achieve 10^4-fold enrichment of target cells relative to leukocytes. In patients with metastatic castration-resistant prostate cancer, where CTCs are not significantly larger than leukocytes, CTCs can be captured based on deformability at 25× greater yield than with the conventional CellSearch system. Finally, the CTCs separated using this approach are collected in suspension and are available for downstream molecular characterization.*

E. S. Park, C. Jin, Q. Guo, R. R. Ang, Dr. S. P. Duffy, Dr. K. Matthews, Prof. H. Ma
Department of Mechanical Engineering
University of British Columbia
2054-6250 Applied Science Lane,
Vancouver, BC V6T 1Z4, Canada
E-mail: hongma@mech.ubc.ca

Dr. A. Azad, Dr. K. N. Chi
BC Cancer Agency–Vancouver Cancer Centre
600 West 10th Avenue, Vancouver, BC V5Z 1L3, Canada

Dr. H. Abdi, Dr. T. Todenhöfer, J. Bazov, Dr. K. N. Chi, Dr. P. C. Black, Prof. H. Ma
Vancouver Prostate Centre
2660 Oak Street, Vancouver, BC V6H 3Z6, Canada

DOI: 10.1002/smll.201503639

1. Introduction

Circulating tumor cells (CTCs) are malignant cells that have escaped from a primary tumor into the bloodstream with the potential to form metastases at anatomically distant sites. Since metastasis contributes to ≈90% of cancer related deaths, CTCs are likely to provide tumor biomarkers for (1) estimation of patient survival,[1–4] (2) development of personalized therapy,[2,5] (3) rapid evaluation of new drugs in clinical trials,[6] and (4) characterization of metastatic disease without the need for tissue biopsy.[7,8]

The key challenge in the separation and analysis of CTCs from patient blood is their extreme rarity, where there are as few as one CTC in 1 mL of whole blood. This needle-in-a-haystack problem is typically dealt with by specific

enrichment of CTCs based on their immunological phenotype, such as epithelial cell adhesion molecule (EpCAM) antigen expression,[9–12] followed by evaluation by immunofluorescence microscopy.[13–15] However, the effectiveness of EpCAM immunoaffinity enrichment has come into question because of the phenotypic switch associated with epithelial–mesenchymal transition (EMT) of tumor cells during metastasis. Post-EMT CTCs exhibit reduced expression for epithelial biomarkers such as EpCAM.[16–19] Recognizing that these aggressively metastatic cells are likely to evade capture by EpCAM immunoaffinity enrichment has prompted significant interest in developing label-free CTC enrichment strategies.

Pathologists have long claimed to be able to identify CTCs using direct microscopic observation of blood.[20] A key discriminating morphological feature of epithelium-derived CTCs is their greater size relative to hematological cells, which has inspired the development of a range of size-based CTC enrichment strategies, including hydrodynamic chromatography,[21] inertial flow,[22–24] acoustophoresis,[25–27] dielectrophoresis,[28] and filtration of fixed cell samples.[29] However, significant pleomorphism is observed in CTCs derived from some tumors, such as prostate and colorectal cancer, where CTCs may overlap significantly with the size of leukocytes.[30–34]

One approach to improve the selectivity of size-based separation methods is to distinguish CTCs from leukocyte based on cell deformability. Tumor cells develop an enlarged nucleus and are therefore likely to exhibit a greater nucleus-to-cytoplasm ratio than leukocytes.[32,33,35,36] In fact, the nucleoplasm is three to four times more rigid and nearly two times more viscous than the cytoplasm.[37] Existing approaches that distinguish CTCs from leukocytes primarily on the basis of deformability typically involve filtration using micropores formed using perforated plastic tape,[38] polycarbonate membranes,[39,40] and photolithographically defined microstructures.[41–43] A key challenge for these devices is clogging and adsorption, which degrades the selectivity of the process and limit the ability to extract the separated cells for subsequent analysis. Specifically, the accumulation of cells in the filter microstructure increases in the hydrodynamic resistance of the filter (Video S1, Supporting Information), and consequently, the filtration force applied to each cell. Modifying the filtration pressure cannot adequately compensate for changes in the filter hydrodynamic resistance because the cell capture process is essentially stochastic. Additionally, increasing the filtration pressure greatly increases the likelihood of rupturing the cells while they transit the filter. Finally, prolonged contact between the filter microstructure and the captured cells often results in irreversible adsorption, which significantly limits the ability to extract the separated cells for downstream characterization.

Here, we developed a microfluidic device capable of deformability-based separation of CTCs using continuous oscillatory flow through a matrix of tapered constrictions. The key novelty of this mechanism is the ability to deform cells in continuous flow in order to alter its flow path without needing to accumulate cells in the separation microstructure. Since cells do not accumulate within the separation microstructures, the hydrodynamic resistance remains relatively constant, which preserves the selectivity of the separation process. We show this approach is capable of directly fractionating whole blood to perform highly selective separation of CTCs based on deformability. Even when CTCs and leukocytes are similarly sized, as observed in prostate cancer, deformability-based separation improves selectivity by 20× to 100× relative to size-only separation. In tandem analysis, we demonstrate that this system is able to isolate 25× more CTCs than the established CellSearch system, while the separated cells remain in suspension and are available for downstream characterization.

The separation mechanism presented here derives from our previous work on the microfluidic ratchet mechanism, where we showed the deformation of individual cells through tapered constrictions is directionally asymmetric, as well as the potential to use this effect for cell separation.[44–46] In our original realization, however, the cells must be processed in small batches, which dramatically limited the throughput of the process to ≈9000 cells per hour, which is impractical for dealing with the large number of cells in whole blood. Here, we developed a continuous process that increased throughput ≈500× to enable deformability-based separation of CTC directly from whole blood.

2. Results

2.1. Principle of Continuous Filtration Using Microfluidic Ratchets

The microfluidic ratchet mechanism relies on the deformation of single cells through funnel-shaped constrictions where the opening of the constriction is smaller than the diameter of the cell. Deforming cells along the direction of the funnel requires less force than against the direction of the funnel. Therefore, oscillatory flow of an appropriate magnitude can cause cells of a specific size and deformability (or more precisely, squeezability) to ratchet through the funnel (Video S2, Supporting Information).[44,46,47] Deformability-based cell separation can be achieved when more deformable cells ratchet through the funnel constriction while less deformable cells are blocked by the constrictions and then released with each flow reversal (**Figure 1**A,B).

To separate a large number of cells, this process is performed continuously using a 2D array of funnel constrictions where the size of the funnel opening is gradually reduced from the bottom row to the top row (Figure 1C). Microchannels lining the top and bottom of the funnel array provide a biased oscillatory flow, while microchannels lining the left of the funnel array provide a constant rightward flow. Cells are infused from the bottom-left of the funnel array and proceed to travel in a zigzag diagonal path until reaching a blocking funnel row, where they proceed horizontally toward the outlet reservoirs (Figure 1C). Cells do not experience significant deformation until nearing their blocking funnel row, where the ratchet effect permits them to transit only unidirectionally. After reaching the blocking funnel row, the fractionated cells are constrained vertically between two

small 2016,
DOI: 10.1002/smll.201503639

small NANO MICRO

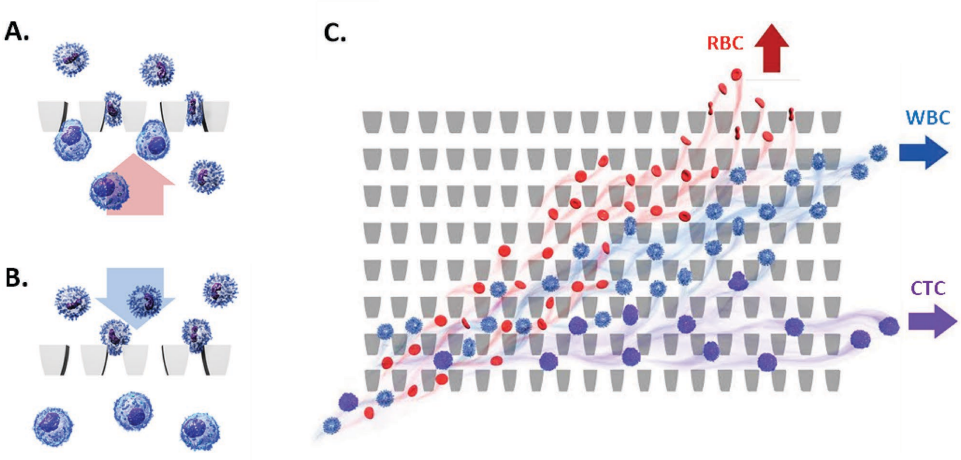

Figure 1. A,B) Principle of the microfluidic ratchet mechanism where oscillatory flow through tapered microscale constrictions allows deformable cells to be transported unidirectionally, while more rigid cells are captured and then released. C) Continuous deformability-based cell separation using oscillatory diagonal flow through a matrix of funnel constrictions. The cell sample is infused into the bottom-left corner of the constriction and propelled by a biased oscillatory flow from the oscillation inlets and a constant rightward flow from the buffer inlet. The infused cells proceed in a zigzag diagonal pattern across the funnel matrix. Highly deformable RBCs pass through the top of the funnel matrix. CTCs and leukocytes proceed diagonally until reaching a blocking funnel row where they proceed horizontally toward separate outlets.

funnel rows, enabling them to be extracted using a constant rightward flow. Red blood cells (RBCs) are not constrained by the funnel constrictions because of their extreme deformability. Consequently, they follow the bulk fluid and flow diagonally into the microchannels lining the top of the funnel array (Figure 1C, Video S3, Supporting Information).

The combination of oscillatory flow and asymmetrical deformation enables perpetual reuse of the filtration microstructures to perform a continuous separation process. Since the cells come into contact with the filtration microstructures only momentarily, clogging and adsorption is effectively eliminated even for high-density samples like whole blood (Video S3, Supporting Information). Additionally, because target cells are not trapped by the filter microstructure during the separation process, the hydrodynamic resistance of the filter remains constant, which allows all incoming cells to experience a constant filtration force (Video S4, Supporting Information). A significant advantage of the continuous filtration mechanism is that it provides direct processing of whole blood without requiring any prior sample preparation, which greatly simplifies process and reduces loss of potential target cells.

2.2. Tapered Constriction Design and Modeling

The structure of the tapered constrictions is set by three parameters shown in **Figure 2**A: the thickness of the microchannel (H), the pore size (W_0), and the shape of the funnel taper ($f(x)$). The thickness of the microchannel is selected to allow cells to expand vertically as they are deformed laterally to provide stress relief. These capabilities are essential for preventing cells from rupturing as they are deformed. For blood cells and cancer cells, a thickness of 30 µm or greater was experimentally determined to be sufficient. The pore size is defined as the opening of the constriction, which varies from 2–18 µm in the CTC separation device. The pressure required to deform cells through each constriction depends on a combination of the pore size and the shape of the funnel taper, which also provides the directional asymmetry responsible for the microfluidic ratchet effect.

A simple method to model the deformation of single cells through a constriction is to consider the cell as an idealized liquid drop held together by a surface tension T_0.[48] Since single cells are deformed laterally, but are unconstrained vertically, the deformation pressure required to push such an ideal liquid drop through a constriction can be determined using Laplace's law

$$\Delta P = T_0 \left(\frac{1}{R_a} - \frac{1}{R_b}\right) \quad (1)$$

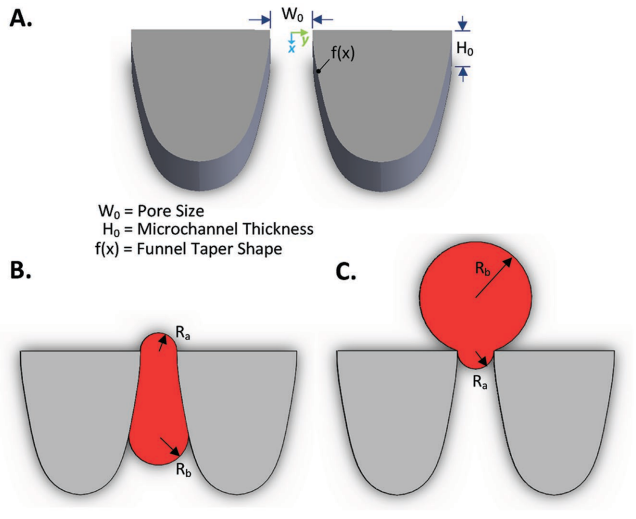

Figure 2. A) The structure of the tapered constriction is determined by the parameters of microchannel thickness (H_0), pore size (W_0), and funnel taper shape ($f(x)$). B,C) Modeling single cell as a liquid drop to estimate its deformation pressure along and against the direction of taper.

DOI: 10.1002/smll.201503639

where ΔP is the pressure difference required to push a cell through the constriction, while R_a and R_b are the effective leading edge and trailing edge radii of the cell. The directional asymmetry of the deformation process can readily be observed using this simple model. Specifically, when a cell transits the constriction along the direction of taper, both the leading edge and the trailing edge are constrained, which reduces the difference between R_a and R_b, resulting in smaller transiting pressure (P_F, Figure 2B). Conversely, when the cell transits the tapered constriction in the reverse direction, only the leading edge is constrained, while the trailing edge is unconstrained, which enlarges the difference between R_a and R_b, resulting in greater transiting pressure (P_R, Figure 2C).[46,49] The difference in deformation pressure between P_F and P_R forms the basis of the ratchet transport phenomenon resulting in three distinct flow paths for each cell when it is transported using oscillatory flow through a series of constrictions with decreasing pore sizes. Specifically, 1) if $\Delta P < P_F$, the cell is blocked by the constriction; 2) if $P_F < \Delta P < P_R$, the cell is ratcheted through the constriction until it reaches a constriction small enough where it gets blocked; and 3) if $\Delta P > P_F$, the cell follows the fluid flow eventually exiting the funnel array, which is exactly the case for red blood cells.

In a previous study, we investigated the deformation pressure asymmetry as a function of the funnel shape for both straight and curved tapers. Not surprisingly, we found that the deformation pressure required for the same cell to transit along the direction of taper was smaller for more gradual tapers than more abrupt tapers.[46] However, gradual tapers also applied significantly greater compression to each cell, which greatly increased the potential for rupture.[44] To obtain a gradual taper while minimizing cell compression, we used a curved taper with the parabolic profile, $y = kx^2 + W_0/2$, where $k = 2000\ m^{-1}$. A curved funnel taper has the additional benefit of reducing the occurrence of sharp corners, which may be challenging to replicate reliably using photolithographic microfabrication.

2.3. Microfluidic Device Design for CTC Separation

The separation of CTCs from whole blood is performed using a matrix of tapered constrictions consisting of 32 rows and 2048 columns. The pore size of the constrictions is kept constant along each row and decreases, from 18 to 2 μm, from the bottom to the top of the matrix. When whole blood is infused into the bottom-left corner of the matrix, fluid flow carries cells in a zigzag diagonal path from the bottom-left to the top-right of the constriction matrix. The RBCs flow to the top of the matrix and exit through the top oscillation channel because they are undeformed by the funnel constrictions. The leukocytes and CTCs flow until reaching their respective limiting constriction sizes where they proceed rightward (Video S3, Supporting Information). CTCs and leukocytes are specifically discriminated across a row of 6 μm constrictions, where cells that deform past this cut-off row are collected in the leukocyte outlet, while cells that fail to deform past the cut-off row are collected into the CTC outlet. The threshold deformation pressure at the cut-off row (ΔP_{cutoff}) can be estimated from the total flow rate through the cut-off constriction row (Q) and their hydrodynamic resistance (R_{cutoff}) using the equation

$$\Delta P_{cutoff} = Q \times R_{cutoff} \quad (2)$$

Oscillatory flow through the cut-off row is generated using pressure-driven flow originating from the oscillation flow channel. Similarly, the constant buffer flow orthogonal to the oscillatory flow is generated using pressure-driven flow originating from the buffer and sample inlets. To ensure the flow rates remain constant irrespective of the hydrodynamic resistance of the constriction array, the hydrodynamic resistance of the supporting microchannels is designed to be significantly greater than the hydrodynamic resistance of the constriction matrix. The specific selectivity for capturing tumor cells can be adjusted from the pressure applied at the oscillation inlet, while the path taken by the cell sample through the constriction matrix can be adjusted from the relative pressure at the oscillation and buffer inlets. The throughput for processing whole blood is approximately 1 mL per hour and can vary depending on the viscosity of the blood and the pressure applied at the sample, buffer, and oscillation inlets. Optimization of these parameters is discussed in the next section.

2.4. Device Validation Using Tumor Cells Doped into Whole Blood

The ability to separate cancer cells from whole blood was initially tested by doping UM-UC13 bladder cancer cells into whole blood. Tumor cells and leukocytes were fluorescently labeled to observe them in transit through the sorting region and to enumerate them in the collection outlets. We confirmed the diagonal path taken by leukocytes and cancer cells upon reaching their limiting funnel size (**Figure 3**; Video S3, Supporting Information). Specifically, both tumor cells and leukocytes follow a diagonal path until reaching a limiting funnel size, at which point they follow a horizontal path through the constriction matrix. Whereas erythrocytes are unconstrained by the constriction matrix and exit from the top of the matrix into the oscillation channel. The capture rate and enrichment ratio of tumor cells can be tuned by adjusting the pressure applied at the oscillation inlet. Specifically, we performed experiments at a doping ratio of one tumor cell to 1000 leukocytes to study the parameters relevant to the separation of rare cells. Enrichment ratio can be varied from 5000 to 14 000 when the pressure applied across the cut-off funnel row is varied from 31 to 46 kPa (**Figure 4**A). Simultaneously, the tumor cell capture rate can be varied from 90% to 77% over the same range (Figure 4B). Varying the cancer cell to leukocyte doping ratio from 1:238 to the more biologically relevant value of $1{:}2.4 \times 10^4$, while operating at the oscillation pressure of 30 kPa, increases the enrichment ratio from 1900 to 8500. Under these parameters, the capture rate remains relatively

DOI: 10.1002/smll.201503639

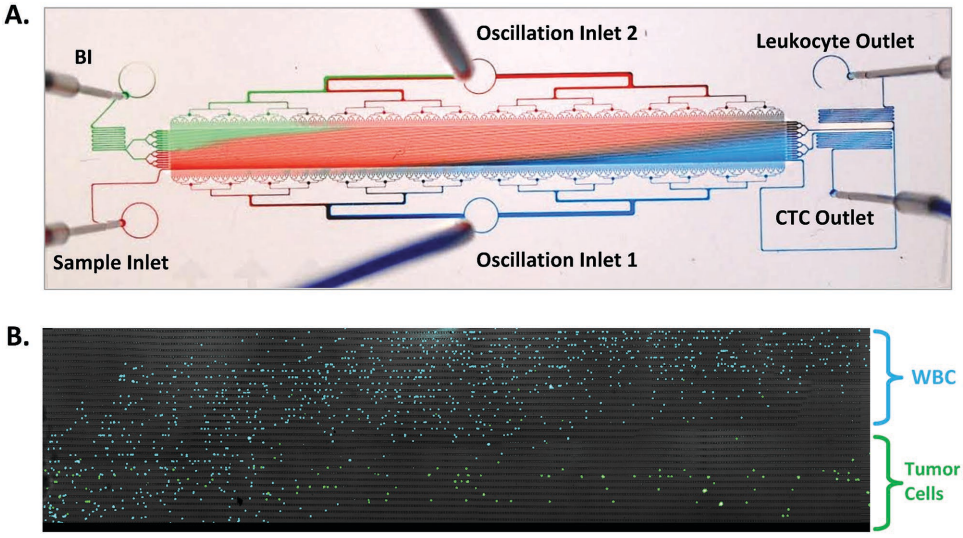

Figure 3. A) Photograph of the microfluidic ratchet device infused with colored water to show the diagonal flow pattern in the separation matrix. B) Composite fluorescence image of leukocytes (blue) and doped UM-UC13 cancer cells (green) in the funnel matrix during a separation process. The leukocytes follow an approximate diagonal path until reaching a limiting funnel size, while doped UM-UC13 cells are limited below the 6 μm funnel row.

constant between 93% and 96%, with the slightly reduced capture rate at 1:1000 doping ratio likely arising from the crowding of the constriction matrix by the larger number of tumor cells (Figure 4C,D).

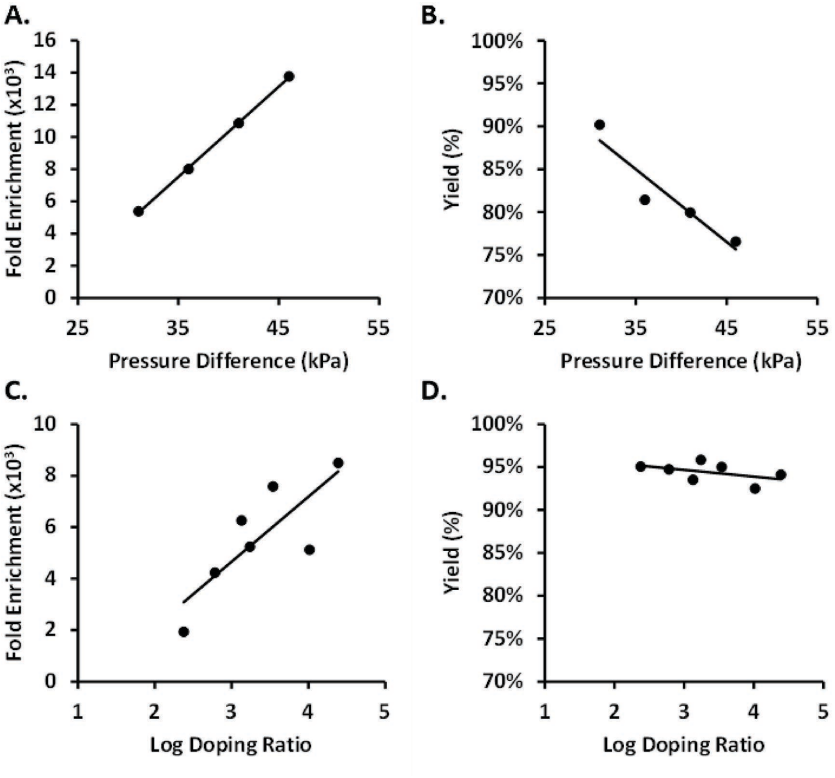

Figure 4. A,B) Performance of deformability-based separation of UM-UC13 cancer cells doped into whole blood at the cancer cell to leukocyte ratio of 1:1000. Enrichment and yield are characterized as a function of deformation pressure (at the 6 μm cutoff funnels). C,D) Relationship of doping ratio and deformability-based system performance. Enrichment and yield are characterized as a function of doping ratio of cancer cells to leukocytes.

2.5. Improving Selectivity through Deformability-Based Cell Separation

To quantify the improvement in selectivity provided by deformability-based separation over simple size-based separation, we measured the size distribution of leukocytes and doped UM-UC13 cancer cells (**Figure 5**A). Assuming the cells are immutable spheres that follow a normal distribution, the theoretical enrichment for an ideal size-only separation process could be determined. Compared to empirical results obtained using the microfluidic ratchet device, size and deformability-based separation improves enrichment by 18× to 100× at a capture rate of 77% to 90%, respectively (Figure 5B). The ability to enrich CTCs based on deformability is advantageous because the size of CTCs may exhibit significant overlap with the size of contaminant leukocytes.[31,32,50]

2.6. Viability and Proliferative Capacity of Enriched Cells

To verify the viability of the separated tumor cells, we performed the MTT assay. UM-UC13 cell suspensions with at least 98% viable cells were enriched by microfluidic ratchet and the cells extracted from the device outlet retained 99.1% viability, relative to these pre-enriched cells. Furthermore, enriched cells showed comparable proliferative capacity and MTT assay indicated that the cells show similar

DOI: 10.1002/smll.201503639

www.MaterialsViews.com

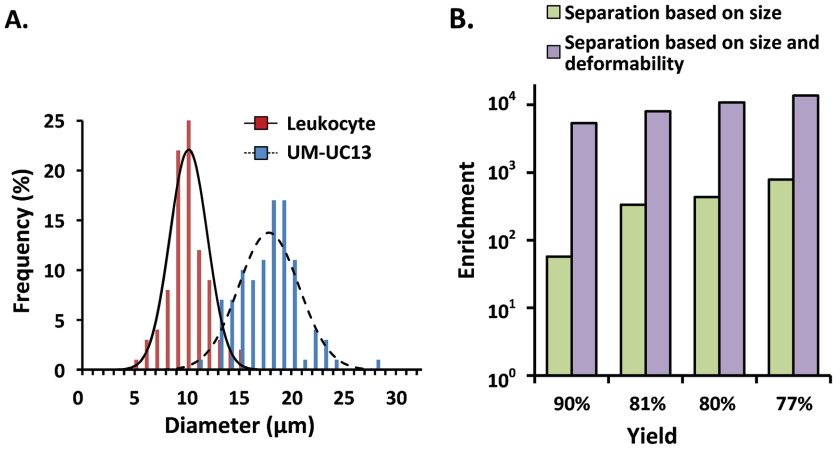

Figure 5. A) Size distribution of leukocytes and UM-UC13 cancer cells. B) Enrichment of doped UM-UC13 cancer cells obtained through deformability-based separation using the microfluidic ratchet device compared to the optimal performance obtained through size-only separation calculated from cell size distribution in (A).

metabolic activity, compared to the pre-enriched population (**Figure 6**).

2.7. Separation of CTCs from Patients with Castrate Resistant Prostate Cancer

To evaluate the ability to separate patient-derived CTCs directly from whole blood, we sampled blood from 20 patients with metastatic castrate-resistant prostate cancer (mCRPC) and four healthy control donors. For each individual, 2 mL of blood were processed by the microfluidic device and 7.5 mL were processed using the CellSearch system. The enriched sample were stained for DNA content (4,6-diamidino-2-phenylindole, DAPI), epithelial markers EpCAM and cytokeratins 8 and 18 (CK), as well as the leukocyte marker CD45 (**Figure 7**A). CTCs were identified on the basis of an intact nucleus, expression of CK, and the absence of expression of the leukocyte marker CD45. Since significant variability existing in the expression level of these markers are known to exist in CTCs,[51,52] we used multispectral imaging (Zeiss LSM 780) to supplement standard fluorescence microscopy in order to provide a more objective method to identify CTCs. This approach collects spectroscopic information from each pixel of a fluorescence image to provide effective unmixing of different fluorochromes to minimize bleed-over between fluorescence spectra. In the current study, cells were considered as a CTC only if they conformed to the morphological and immunofluorescence criteria ($CK^+CD45^-DAPI^+$) by visual inspection and also have clearly distinct fluorescence maxima for each fluorophore (Figure 6B).

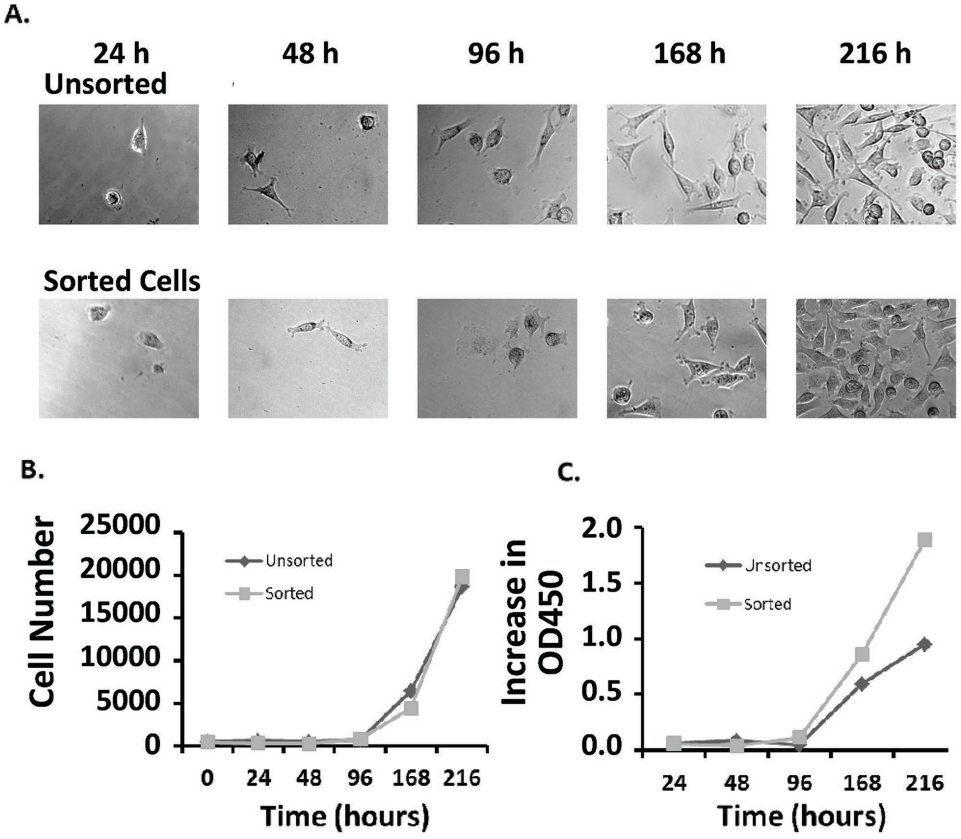

Figure 6. A) Cell density of UM-UC13 cells, transferred directly to culture media after microfluidic ratchet enrichment. B) Measurement of cell number, during subsequent culture. C) Assessment of cell metabolic activity based on MTT assay.

small 2016,
DOI: 10.1002/smll.201503639

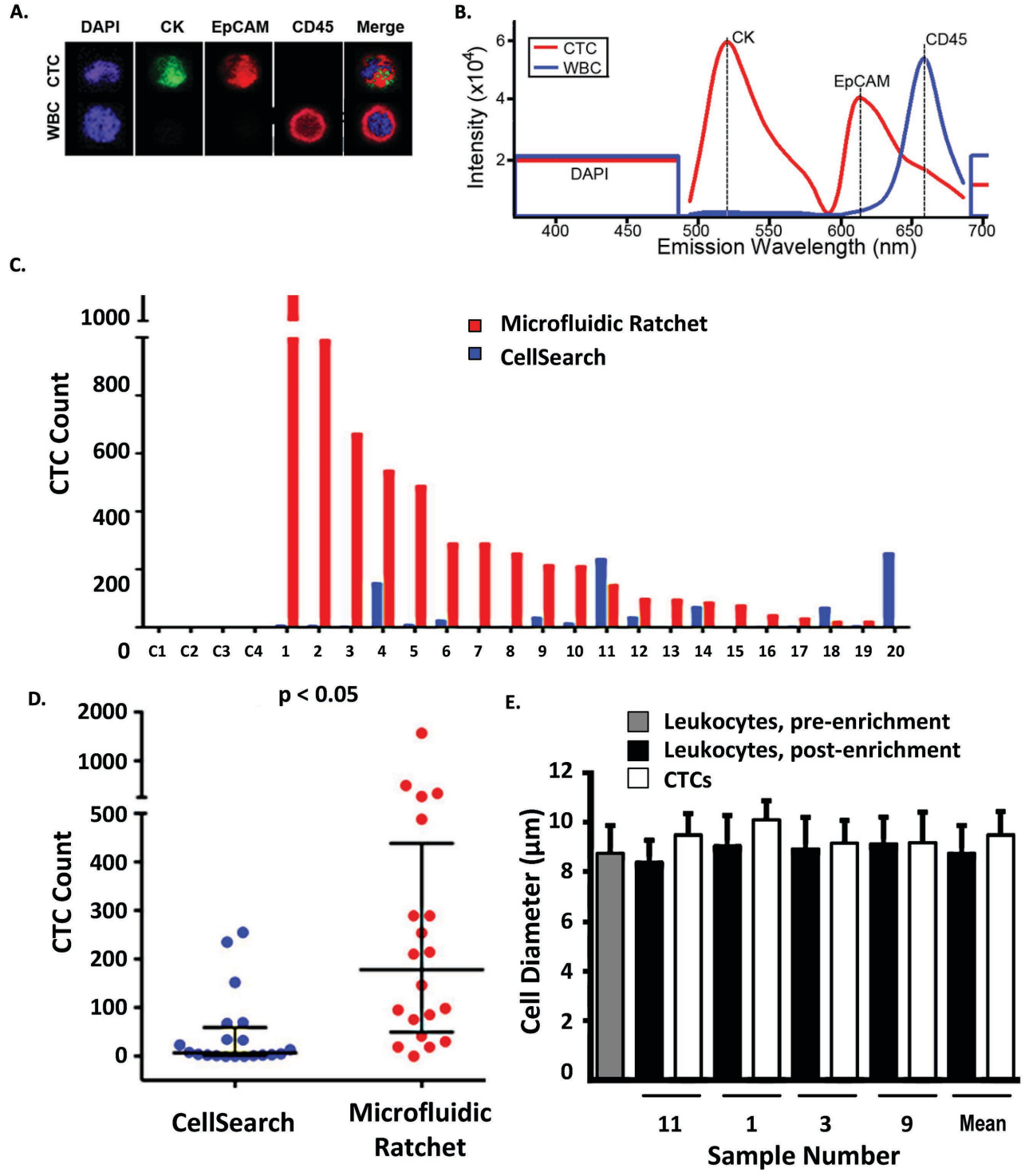

Figure 7. A,B) Fluorescence microscopy image and corresponding spectra for CTCs ($DAPI^+CK^+CD45^-$) and leukocytes ($DAPI^+CK^-CD45^+$). C,D) CTC enumeration from four controls and 20 patients with metastatic castrate-resistant prostate cancer performed using the microfluidic ratchet device and the CellSearch system. The *p*-value indicates a significant difference by Wilcoxon-ranked sum. E) Comparison of cell size between leukocytes and CTCs derived from four patient-derived samples, which showed no statistically significant difference.

Based on this criterion, CTC enumeration from immunofluorescence images was performed by multiple blinded individuals. The microfluidic ratchet system was significantly more sensitive in detection of CTCs with a median 178 CTCs/7.5 mL compared to a median 7 CTCs/7.5 mL detected by CellSearch (Figure 7C,D; $p = 0.0031$). Interestingly, the number of CTCs detected following microfluidic enrichment did not correlate with the number detected by CellSearch. This discordance likely derives from the fact the biophysical separation is likely to access a different population of CTCs than immunomagnetic enrichment used by CellSearch.

DOI: 10.1002/smll.201503639

To investigate the potential for false positives, we performed experiments using blood from four healthy donors, where we found a median of 4 false-positive cells/7.5 mL. The existence of false positives is a common feature of all CTC identification methods, including the CellSearch system. These cells potentially arise from epithelial cells sloughed into blood from venipuncture or tissue trauma, or from the expression of cytokeratins in leukocytes.[53] While the presence of false positives limits the ultimate specificity of the system, the number of false positives was significantly lower than the median CTC number in patient samples.

Label-free enrichment of CTCs from patients with prostate cancer presents a challenge because these CTCs tend to have cell diameters that overlap significantly with that of leukocytes.[31,32,50] Based on our model we predicted that, while the microfluidic ratchet mechanism sorted by size and deformability, the selectivity of the system was predominantly due to deformability-based sorting. Therefore deformability-based sorting would permit selective enrichment of CTCs from leukocytes of similar size. To evaluate this capability, we measured the diameter of enriched CTCs, as well as the diameter of patient leukocytes before and after enrichment. Consistent with our hypothesis, the contaminating leukocytes in the collection outlet were not significantly larger than the pre-enriched population. Furthermore, there was significant overlap in size between CTCs and leukocytes, suggesting that these cells were primarily discriminated on the basis of their cell deformability (Figure 7E).

3. Discussion

Deformability-based cell sorting is particularly relevant to the separation of CTCs from whole blood where CTCs may not be easily discriminated from leukocytes based on size alone. This situation is particularly relevant for prostate and colorectal cancer where patient-derived CTCs are known to be smaller and have significant size overlap with contaminant leukocytes.[31,32,50] Here, we show that deformability-based separation improves enrichment ≈100× over size-only separation, providing a highly selective biophysical enrichment process. This capability is especially important when considering downstream genetic profiling of the separated CTC sample to stratify cancer patients or to evaluate disease progression and drug efficacy.[54–57] Genotyping CTCs in these applications require samples with high purity since contaminate leukocytes could easily confound genetic and gene expression profiling.[56,57] Since biophysical separation processes are inherently orthogonal to biochemical separation processes, these approaches could be combined to multiplicatively improve selectivity in order to provide samples with greater purity.

Another key insight emerging from this study is how principles associated with natural ratchet mechanisms can be used in biophysical cell sorting. Molecular scale ratchet mechanisms involve the coupling of a physical asymmetry with stochastic background energy.[58,59] These mechanisms are found ubiquitously in nature to deterministically transport molecules and subcellular components against the overwhelming viscous background of their fluid environment. In this work, we showed that at the cellular scale, a physical asymmetry and an oscillatory background can be coupled together to deterministically transport cells based on deformability, while providing the benefit of preventing clogging and adsorption to ensure continuous and consistent reuse of the ratchet components.

4. Experimental Section

Microfluidic Device Fabrication: Microfluidic devices were made using polydimethylsiloxane (PDMS) as previously described.[44] Briefly, microstructure patterns were designed using DraftSight (Dassault Systems, Vélizy-Villacoublay, France) and translated onto commercially printed optical photomasks (Advanced Reproductions, Andover, MA). One high-resolution photomask was used to generate the microscale funnel constrictions while one low-resolution photomask was used for the flow channels. An inverse master of the device was fabricated on a silicon wafer with two silicon layers. The first layer was the silicon wafer layer comprising the central sorting area. This silicon wafer was coated with epoxy-based negative photoresist SU-8 8025 (Microchem, Newton, MA), spun at 3000 rpm for 30 s to produce a 30 μm thick layer. The wafer was then baked at 95 °C for 5 min and exposed to UV light through the optical photomask. After exposure, the patterned wafer was baked at 65 °C (1 min), 95 °C (4 min), and 65 °C (1 min), and washed with isopropanol. The second layer formed the flow channels and aligned with the photomask with the first pattern. The second set of SU-8 features was patterned as described above, with a spin speed of 2200 rpm for 30 s. This resulted in microstructures 40 μm in height and the structures were hardened by ramping the temperature from 40 °C to 165 °C, at increments of 15 °C/10 min. The device was then incubated 165 °C for 30 min and cooled to 65 °C by ramping the temperature by 50 °C/10 min. The final heights of the first and second layer were measured to be 29.6 and 40.1 μm, respectively. The PDMS device was subsequently attached to a glass slide by 90 s of activation in air plasma (Harrick Plasma, Ithaca, NY). The PDMS device was subsequently attached to a glass slide by 90 s of activation in air plasma (Harrick Plasma, Ithaca, NY).

Microfluidic Device Fabrication and Operation: Cell separation processes involved initially filling the microfluidic device using phosphate buffered saline (PBS) with 0.2% Pluronic F127 (Invitrogen) to prevent nonspecific adsorption of cells to the wall of the device. Whole blood samples were infused through the device through the sample inlet, while buffer solutions were infused through the buffer and oscillation inlets. Pressure-driven flow originating from these inlets was controlled using a commercial pressure controller (Fluigent, Paris, France), as well as a custom-made pressure control system and software described previously.[33] The throughput for processing whole blood was approximately 1 mL per hour per device. Typically, two microfluidic devices were run in parallel.

Tumor Cell Doping Experiments: The UM-UC13 bladder cancer cell line, provided by Pathology Core of the Bladder Cancer SPORE at MD Anderson Cancer Center, was cultured in minimum essential media (MEM), supplemented with fetal bovine serum (10% v/v), 1% l-glutamine, 1% MEM nonessential amino acids, and 1%

DOI: 10.1002/smll.201503639

sodium pyruvate (Invitrogen), as well as 1% penicillin-streptomycin (Fisher Thermo Scientific, Waltham, MA). The cells were cultured in a humidified incubator at 37 °C and 5% CO_2.

UM-UC13 cells were doped into 5 mL whole blood at a ratio of 1 tumor cell to 1000 leukocytes, except where indicated otherwise, and processed using the microfluidic ratchet device. Following the separation process, the collection reservoir was imaged to determine yield, enrichment, and purity by counting the relative number of Calcein AM Green labeled UM-UC13 versus Hoechst 33342-labeled leukocytes. The parameters for yield, enrichment, and purity are defined as follows

$$\text{Percent Yield} = 100\% \times \frac{\text{Target Cells}_{\text{Output}}}{\text{Target Cells}_{\text{Input}}}$$

$$\text{Percent Purity} = 100\% \times \left(\frac{\text{Target Cells}}{\text{Target Cells} + \text{Background Cells}} \right)_{\text{Output}}$$

$$\text{Enrichment} = \frac{(\text{Target Cells}/\text{Background Cells})_{\text{Output}}}{(\text{Target Cells}/\text{Background Cells})_{\text{Input}}}$$

$$\text{Percent Viability} = 100\% \times \frac{\text{No. of Viable Cells at Output}}{\text{No. of Viable Cells at Input}}$$

Viability of the separated UM-UC13 cells was assessed using the LIVE/DEAD assay (Invitrogen) both prior to and after microfluidic enrichment. The enriched cells were subsequently cultured for 10 d to assess the proliferative capacity of the cells.

Assessment of the Role of Cell Deformability in Separation Performance: To measure cell size, the cell samples were suspended in PBS and visualized using an inverted microscope (Ti-U, Nikon, Tokyo, Japan) and CCD camera (DS-2MBW, Nikon, Tokyo, Japan). To estimate the effect of deformability on distribution, the distribution of cell size was measured for UM-UC13 cells and leukocytes. A normal distribution was fitted to each distribution. The cells were then modeled as immutable spheres to estimate how they may be separated based on size alone. Using this model, the predicted yield and enrichment could be established for size-only separation of cells. The empirically derived relationship between target cell yield and enrichment was then compared with this model to determine the performance improvement obtained through deformability-based separation.

Patient Sample Preparation and Processing: Blood samples from mCRPC patient blood ($n = 20$) were collected by venipuncture into 6 mL ethylenediaminetetraacetic acid (EDTA) tubes for processing using the microfluidic ratchet device and 10 mL CellSave tube for CellSearch analysis. For the microfluidic ratchet device, whole blood was processed within 2 h of blood collection. Each microfluidic ratchet device is capable of processing whole blood at a throughput of 1 mL per hour. Typically, two devices were used in parallel to in patient experiments. Additional parallelization can be used to achieve greater throughput. After processing, cells from the CTC reservoir were collected in a 15 mL falcon tube, and then washed using PBS by centrifuging at 400 × *g* for 5 min. The cells were then fixed with 4% of paraformaldehyde (PFA) for 15 min and again washed with PBS. Next, the cells were permeabilized with 0.025% of Tween20 for 10 min, washed with PBS, and blocked with 3% bovine serum albumin (BSA) in PBS for 1 h. The antibody cocktail, consisting of CK-Alexa 488, EpCAM-Alexa594, and CD45-allophycocyanin (APC), were then added and incubated at 4 °C overnight. Finally, the cells were washed with PBS twice, counter stained with DAPI, and transferred to 384 optically transparent well plate (Corning) for microscopy to identify CTCs using the process described below.

CTC Identification: The enriched CTC sample were extracted from the collection reservoir and stained with anti-pan-cytokeratin antibody conjugated with Alexa 488 (CellSignaling), anti-EpCAM antibody conjugated with Alexa 584 (CellSignaling), and anti-CD45 antibody conjugated with APC (Biolegend), and counter stained for DAPI (Vector Lab). Stained cells were transferred to a 384-well optically transparent plate (Corning), and scanned with Ziess LSM 780 system. The entire well was imaged under a 40× oil immersion objective over 15 × 15 frames using a motorized stage. Each captured image consisted of a 34 color spectral image including a transmission-photomultiplier (T-PMT) channel (bright field), a low-wavelength PMT channel (DAPI), and 32 channels captured using a GaAsP spectral detector (CK/EpCAM/CD45).

The process to identify CTCs from the spectral image involved first scanning for cells that showed bright green fluorescence indicating the presence of CK, without ring-shaped fluorescence emitted by CD45 on the cell surface. Each candidate CTC was then carefully analyzed using a region-of-interest capture of the spectral data of pixels encapsulating each candidate cell. CTCs were specifically classified based on an emission maximum at 521 nm (pan-keratin conjugated Alexa 488) with clear DAPI signal and intact membrane shape from bright field image. All CTCs fitting this characteristic also showed a distinct peak at 618 nm for EpCAM. Leukocytes were classified with a spectral maximum at 660 nm (CD45 conjugated with APC). CTC counts obtained from 2 mL of patient blood using the microfluidic ratchet device were scaled to 7.5 mL to compare with results obtained using the CellSearch system.

The size of CTCs and leukocytes from mCRPC patients were measured from the bright field image of the separated cells in suspension by drawing a circle on the outer edge of each target cells. At least 25 CTCs and leukocytes were measured for each mCRPC data set shown in Figure 7E.

CellSearch Analysis: The CellSearch system processed 7.5 mL of mCRPC patient blood samples within 96 h of collection. This system first enriched CTCs using Anti-EpCAM magnetic beads, and labeled the enriched cells using DAPI, CK-phycoerythrin (PE), and CD45-APC. The enriched cells were deposited in the CellTracks Magnet, and imaged using the CellTracks Analyzer. Finally, a certified technician at the Clinical Assay Laboratory at Vancouver Prostate Centre visually reviewed the candidate cells to identify CTCs defined as DAPI+CK+CD45-cells.

Supporting Information

Supporting Information is available from the Wiley Online Library or from the author.

DOI: 10.1002/smll.201503639

Acknowledgements

The authors would like to acknowledge funding support from the Canadian Institutes of Health Research, Natural Science and Engineering Research Council of Canada, Prostate Cancer Canada, Vancouver Prostate Centre's Translational Research Initiative for Accelerated Discovery and Development, C. J. Martin Biomedical Overseas Fellowship from the National Health and Medical Research Council of Australia, and the Engineers-in-Scrubs training program at UBC.

[1] J. S. de Bono, H. I. Scher, R. B. Montgomery, C. Parker, M. C. Miller, H. Tissing, G. V. Doyle, L. W. W. M. Terstappen, K. J. Pienta, D. Raghavan, *Clin. Cancer Res.* **2008**, *14*, 6302.
[2] M. Cristofanilli, G. T. Budd, M. J. Ellis, A. Stopeck, J. Matera, M. C. Miller, J. M. Reuben, G. V. Doyle, W. J. Allard, L. W. M. M. Terstappen, D. F. Hayes, *N. Engl. J. Med.* **2004**, *351*, 781.
[3] G. T. Budd, M. Cristofanilli, M. J. Ellis, A. Stopeck, E. Borden, M. C. Miller, J. Matera, M. Repollet, G. V. Doyle, L. W. M. M. Terstappen, D. F. Hayes, *Clin. Cancer Res.* **2006**, *12*, 6403.
[4] S. J. Cohen, C. J. A. Punt, N. Iannotti, B. H. Saidman, K. D. Sabbath, N. Y. Gabrail, J. Picus, M. Morse, E. Mitchell, M. C. Miller, G. V. Doyle, H. Tissing, L. W. M. M. Terstappen, N. J. Meropol, *J. Clin. Oncol.* **2008**, *26*, 3213.
[5] C. Massard, A. Chauchereau, K. Fizazi, *Ann. Oncol.* **2009**, *20*, 197.
[6] A. H. M. Reid, G. Attard, D. C. Danila, N. B. Oommen, D. Olmos, P. C. Fong, L. R. Molife, J. Hunt, C. Messiou, C. Parker, D. Dearnaley, J. F. Swennenhuis, L. W. M. M. Terstappen, G. Lee, T. Kheoh, A. Molina, C. J. Ryan, E. Small, H. I. Scher, J. S. de Bono, *J. Clin. Oncol.* **2010**, *28*, 1489.
[7] G. Attard, J. F. Swennenhuis, D. Olmos, A. H. M. Reid, E. Vickers, R. A'Hern, R. Levink, F. Coumans, J. Moreira, R. Riisnaes, N. B. Oommen, G. Hawche, C. Jameson, E. Thompson, R. Sipkema, C. P. Carden, C. Parker, D. Dearnaley, S. B. Kaye, C. S. Cooper, A. Molina, M. E. Cox, L. W. M. M. Terstappen, J. S. de Bono, *Cancer Res.* **2009**, *69*, 2912.
[8] S. Maheswaran, L. V. Sequist, S. Nagrath, L. Ulkus, B. Brannigan, C. V. Collura, E. Inserra, S. Diederichs, A. J. Iafrate, D. W. Bell, S. Digumarthy, A. Muzikansky, D. Irimia, J. Settleman, R. G. Tompkins, T. J. Lynch, M. Toner, D. A. Haber, *N. Engl. J. Med.* **2008**, *359*, 366.
[9] S. Nagrath, L. V. Sequist, S. Maheswaran, D. W. Bell, D. Irimia, L. Ulkus, M. R. Smith, E. L. Kwak, S. Digumarthy, A. Muzikansky, P. Ryan, U. J. Balis, R. G. Tompkins, D. A. Haber, M. Toner, *Nature* **2007**, *450*, 1235.
[10] E. Ozkumur, A. M. Shah, J. C. Ciciliano, B. L. Emmink, D. T. Miyamoto, E. Brachtel, M. Yu, P. Chen, B. Morgan, J. Trautwein, A. Kimura, S. Sengupta, S. L. Stott, N. M. Karabacak, T. A. Barber, J. R. Walsh, K. Smith, P. S. Spuhler, J. P. Sullivan, R. J. Lee, D. T. Ting, X. Luo, A. T. Shaw, A. Bardia, L. V. Sequist, D. N. Louis, S. Maheswaran, R. Kapur, D. A. Haber, M. Toner, *Sci. Transl. Med.* **2013**, *5*, 179ra47.
[11] S. L. Stott, C.-H. Hsu, D. I. Tsukrov, M. Yu, D. T. Miyamoto, B. A. Waltman, S. M. Rothenberg, A. M. Shah, M. E. Smas, G. K. Korir, F. P. Floyd, A. J. Gilman, J. B. Lord, D. Winokur, S. Springer, D. Irimia, S. Nagrath, L. V. Sequist, R. J. Lee, K. J. Isselbacher, S. Maheswaran, D. A. Haber, M. Toner, *Proc. Natl. Acad. Sci. USA* **2010**, *107*, p. 18392.
[12] W. J. Allard, J. Matera, M. C. Miller, M. Repollet, M. C. Connelly, C. Rao, A. G. J. Tibbe, J. W. Uhr, L. W. M. M. Terstappen, *Clin. Cancer Res.* **2004**, *10*, 6897.
[13] S. Riethdorf, H. Fritsche, V. Müller, T. Rau, C. Schindlbeck, B. Rack, W. Janni, C. Coith, K. Beck, F. Jänicke, S. Jackson, T. Gornet, M. Cristofanilli, K. Pantel, *Clin. Cancer Res.* **2007**, *13*, 920.
[14] M. C. Miller, G. V. Doyle, L. W. M. M. Terstappen, *J. Oncol.* **2010**, 617421.
[15] D. R. Shaffer, M. A. Leversha, D. C. Danila, O. Lin, R. Gonzalez-Espinoza, B. Gu, A. Anand, K. Smith, P. Maslak, G. V. Doyle, L. W. Terstappen, H. Lilja, G. Heller, M. Fleisher, H. I. Scher, *Clin. Cancer Res.* **2007**, *13*, 2023.
[16] P. Paterlini-Brechot, N. L. Benali, *Cancer Lett.* **2007**, *253*, 180.
[17] B. Willipinski-Stapelfeldt, S. Riethdorf, V. Assmann, U. Woelfle, T. Rau, G. Sauter, J. Heukeshoven, K. Pantel, *Clin. Cancer Res.* **2005**, *11*, 8006.
[18] L. Zhang, L. D. Ridgway, M. A. Wetzel, J. Ngo, W. Yin, D. Kumar, J. C. Goodman, M. D. Groves, D. Marchetti, *Sci. Transl. Med.* **2013**, *5*, 180ra48.
[19] T. M. Gorges, I. Tinhofer, M. Drosch, L. Röse, T. M. Zollner, T. Krahn, O. von Ahsen, *BMC Cancer* **2012**, *12*, 178.
[20] R. F. Alexander, A. I. Spriggs, *J. Clin. Pathol.* **1960**, *13*, 414.
[21] N. M. Karabacak, P. S. Spuhler, F. Fachin, E. J. Lim, V. Pai, E. Ozkumur, J. M. Martel, N. Kojic, K. Smith, P. Chen, J. Yang, H. Hwang, B. Morgan, J. Trautwein, T. A. Barber, S. L. Stott, S. Maheswaran, R. Kapur, D. A. Haber, M. Toner, *Nat. Protoc.* **2014**, *9*, 694.
[22] H. W. Hou, M. E. Warkiani, B. L. Khoo, Z. R. Li, R. A. Soo, D. S.-W. Tan, W.-T. Lim, J. Han, A. A. S. Bhagat, C. T. Lim, *Sci. Rep.* **2013**, *3*, 1259.
[23] K.-A. Hyun, K. Kwon, H. Han, S.-I. Kim, H.-I. Jung, *Biosens. Bioelectron.* **2013**, *40*, 206.
[24] E. Sollier, D. E. Go, J. Che, D. Gossett, S. O'Byrne, W. M. Weaver, N. Kummer, M. Rettig, J. Goldman, N. Nickols, S. McCloskey, R. Kulkarni, D. D. Carlo, *Lab. Chip* **2014**, *14*, 63.
[25] M. Antfolk, C. Antfolk, H. Lilja, T. Laurell, P. Augustsson, *Lab. Chip* **2015**, *15*, 2102.
[26] P. Augustsson, C. Magnusson, M. Nordin, H. Lilja, T. Laurell, *Anal. Chem.* **2012**, *84*, 7954.
[27] P. Li, Z. Mao, Z. Peng, L. Zhou, Y. Chen, P.-H. Huang, C. I. Truica, J. J. Drabick, W. S. El-Deiry, M. Dao, S. Suresh, T. J. Huang, *Proc. Natl. Acad. Sci. USA* **2015**, *112*, 4970.
[28] S. Shim, K. Stemke-Hale, A. M. Tsimberidou, J. Noshari, T. E. Anderson, P. R. C. Gascoyne, *Biomicrofluidics* **2013**, *7*, 011807.
[29] H. K. Lin, S. Zheng, A. J. Williams, M. Balic, S. Groshen, H. I. Scher, M. Fleisher, W. Stadler, R. H. Datar, Y.-C. Tai, R. J. Cote, *Clin. Cancer Res.* **2010**, *16*, 5011.
[30] F. A. W. Coumans, G. van Dalum, M. Beck, L. W. M. M. Terstappen, *PloS One* **2013**, *8*, e61770.
[31] S. T. Ligthart, F. A. W. Coumans, F.-C. Bidard, L. H. J. Simkens, C. J. A. Punt, M. R. de Groot, G. Attard, J. S. de Bono, J.-Y. Pierga, L. W. M. M. Terstappen, *PloS One* **2013**, *8*, e67148.
[32] S. Park, R. R. Ang, S. P. Duffy, J. Bazov, K. N. Chi, P. C. Black, H. Ma, *PloS One* **2014**, *9*, e85264.
[33] D. Marrinucci, K. Bethel, R. H. Bruce, D. N. Curry, B. Hsieh, M. Humphrey, R. T. Krivacic, J. Kroener, L. Kroener, A. Ladanyi, N. H. Lazarus, J. Nieva, P. Kuhn, *Hum. Pathol.* **2007**, *38*, 514.
[34] D. Marrinucci, K. Bethel, D. Lazar, J. Fisher, E. Huynh, P. Clark, R. Bruce, J. Nieva, P. Kuhn, *J. Oncol.* **2010**, *2010*, 861341.
[35] D. C. Lazar, E. H. Cho, M. S. Luttgen, T. J. Metzner, M. L. Uson, M. Torrey, M. E. Gross, P. Kuhn, *Phys. Biol.* **2012**, *9*, 016002.
[36] S. Meng, D. Tripathy, E. P. Frenkel, S. Shete, E. Z. Naftalis, J. F. Huth, P. D. Beitsch, M. Leitch, S. Hoover, D. Euhus, B. Haley, L. Morrison, T. P. Fleming, D. Herlyn, L. W. M. M. Terstappen, T. Fehm, T. F. Tucker, N. Lane, J. Wang, J. W. Uhr, *Clin. Cancer Res.* **2004**, *10*, 8152.
[37] F. Guilak, J. R. Tedrow, R. Burgkart, *Biochem. Biophys. Res. Commun.* **2000**, *269*, 781.
[38] S. H. Seal, *Cancer* **1959**, *12*, 590.

DOI: 10.1002/smll.201503639

[39] I. Desitter, B. S. Guerrouahen, N. Benali-Furet, J. Wechsler, P. A. Jänne, Y. Kuang, M. Yanagita, L. Wang, J. A. Berkowitz, R. J. Distel, Y. E. Cayre, *Anticancer Res.* **2011**, *31*, 427.
[40] G. Vona, A. Sabile, M. Louha, V. Sitruk, S. Romana, K. Schütze, F. Capron, D. Franco, M. Pazzagli, M. Vekemans, B. Lacour, C. Bréchot, P. Paterlini-Bréchot, *Am. J. Pathol.* **2000**, *156*, 57.
[41] S. Zheng, H. Lin, J.-Q. Liu, M. Balic, R. Datar, R. J. Cote, Y.-C. Tai, *J. Chromatogr. A* **2007**, *1162*, 154.
[42] M. Hosokawa, H. Kenmotsu, Y. Koh, T. Yoshino, T. Yoshikawa, T. Naito, T. Takahashi, H. Murakami, Y. Nakamura, A. Tsuya, T. Shukuya, A. Ono, H. Akamatsu, R. Watanabe, S. Ono, K. Mori, H. Kanbara, K. Yamaguchi, T. Tanaka, T. Matsunaga, N. Yamamoto, *PloS One* **2013**, *8*, e67466.
[43] L. S. Lim, M. Hu, M. C. Huang, W. C. Cheong, A. T. L. Gan, X. L. Looi, S. M. Leong, E. S.-C. Koay, M.-H. Li, *Lab Chip* **2012**, *12*, 4388.
[44] S. M. McFaul, B. K. Lin, H. Ma, *Lab Chip* **2012**, *12*, 2369.
[45] B. K. Lin, S. M. McFaul, C. Jin, P. C. Black, H. Ma, *Biomicrofluidics* **2013**, *7*, 034114.
[46] Q. Guo, S. McFaul, H. Ma, *Phys. Rev. E* **2011**, *83*, 051910.
[47] J. Liu, Y. F. Yap, N.-T. Nguyen, *Phys. Rev. E: Stat. Nonlinear Soft Matter Phys.* **2009**, *80*, 046319.
[48] R. M. Hochmuth, *J. Biomech.* **2000**, *33*, 15.
[49] Q. Guo, S. Park, H. Ma, *Lab Chip* **2012**, *12*, 2687.
[50] F. A. W. Coumans, G. van Dalum, M. Beck, L. W. M. M. Terstappen, *PloS One* **2013**, *8*, e61774.
[51] J. Kraan, S. Sleijfer, M. H. Strijbos, M. Ignatiadis, D. Peeters, J.-Y. Pierga, F. Farace, S. Riethdorf, T. Fehm, L. Zorzino, A. G. J. Tibbe, M. Maestro, R. Gisbert-Criado, G. Denton, J. S. de Bono, C. Dive, J. A. Foekens, J. W. Gratama, *Cytometry B Clin. Cytometry* **2011**, *80*, 112.
[52] A. G. J. Tibbe, M. C. Miller, L. W. M. M. Terstappen, *Cytom. Part J. Int. Soc. Anal. Cytol.* **2007**, *71*, 154.
[53] R. Jung, K. Petersen, W. Krüger, M. Wolf, C. Wagener, A. Zander, M. Neumaier, *Br. J. Cancer* **1999**, *81*, 870.
[54] E. Heitzer, M. Auer, C. Gasch, M. Pichler, P. Ulz, E. M. Hoffmann, S. Lax, J. Waldispuehl-Geigl, O. Mauermann, C. Lackner, G. Höfler, F. Eisner, H. Sill, H. Samonigg, K. Pantel, S. Riethdorf, T. Bauernhofer, J. B. Geigl, M. R. Speicher, *Cancer Res.* **2013**, *73*, 2965.
[55] A. A. Powell, A. H. Talasaz, H. Zhang, M. A. Coram, A. Reddy, G. Deng, M. L. Telli, R. H. Advani, R. W. Carlson, J. A. Mollick, S. Sheth, A. W. Kurian, J. M. Ford, F. E. Stockdale, S. R. Quake, R. F. Pease, M. N. Mindrinos, G. Bhanot, S. H. Dairkee, R. W. Davis, S. S. Jeffrey, *PloS One* **2012**, *7*, e33788.
[56] A. M. Sieuwerts, J. Kraan, J. Bolt-de Vries, P. van der Spoel, B. Mostert, J. W. M. Martens, J.-W. Gratama, S. Sleijfer, J. A. Foekens, *Breast Cancer Res. Treat.* **2009**, *118*, 455.
[57] D. A. Smirnov, D. R. Zweitzig, B. W. Foulk, M. C. Miller, G. V. Doyle, K. J. Pienta, N. J. Meropol, L. M. Weiner, S. J. Cohen, J. G. Moreno, M. C. Connelly, L. W. M. M. Terstappen, S. M. O'Hara, *Cancer Res.* **2005**, *65*, 4993.
[58] E. M. Purcell, *Am. J. Phys.* **1977**, *45*, 3.
[59] J. C. M. Gebhardt, A. E. M. Clemen, J. Jaud, M. Rief, *Proc. Natl. Acad. Sci. USA* **2006**, *103*, 8680.

Received: December 1, 2015
Revised: January 6, 2016
Published online: